PHYSICAL REVIEW A VOLUME 23, NUMBER 3 MARCH 1981

Density-dependent excitation rate for the $2p^2\,{}^3P$ dielectronic satellite line in a laser-produced carbon plasma

J. F. Seely, R. H. Dixon, and R. C. Elton
Naval Research Laboratory, Washington, D.C. 20375
(Received 13 August 1980)

The relative intensities of the $2l2l'$ dielectronic satellite transitions of C v have been measured as functions of electron density and temperature in a laser-produced plasma. The relative intensity of the $2p^2\,{}^3P$-$1s2p\,{}^3P$ transition is observed to vary with electron density in the range 8×10^{19} to 2×10^{20} cm^{-3}. In this density range, the satellite line intensities are consistent with electron collisional population of the $2p^2\,{}^3P$ level from the $2s2p\,{}^3P$ level, both doubly excited. The measured rate coefficient for this collisional transition, inferred from the density dependence of the $2p^2\,{}^3P$ spectral radiation, agrees with recently calculated values. In contrast to previous higher-Z experiments, electron collisional population of the $2p^2\,{}^3P$ level from the singly excited $1s2p\,{}^3P$ level is found to be unimportant in this experiment.

I. INTRODUCTION

Dielectronic satellite spectral lines from highly charged ions are prominent features in the spectra of hot plasmas. These spectral lines result from the radiative decay of doubly excited levels which are normally populated by dielectronic recombination. The radiative transitions from the $2l2l'$ doubly excited levels of heliumlike ions have been identified in spectra from dense laser-produced plasmas.[1-7] The $2p^2\,{}^3P$ spectral radiation, expected to be unobservable due to the negligible dielectronic recombination rate for this level, was found to be anomalously intense. This high intensity has been attributed to two different electron collisional population mechanisms for the $2p^2\,{}^3P$ level: excitation from the $1s2p\,{}^3P$ level[3] (a $\Delta n=1$ transition) and from the $2s2p\,{}^3P$ level[8] (a $\Delta n=0$ transition). A knowledge of the appropriate population mechanism for the $2p^2\,{}^3P$ level is important if this line intensity is to be used as a density diagnostic.[8-11] If the dominant excitation is by a $\Delta n=1$ transition, the other satellite lines could also be similarly excited, so that a study of the $2p^2\,{}^3P$ decay has broad implications for the entire satellite spectrum.

In this paper, we report the measurement[12] of the density dependence of the $2p^2\,{}^3P$-$1s2p\,{}^3P$ spectral line of C V in a laser-produced carbon plasma. Particular attention is paid to the population mechanism of the upper level. In the plasma region near the target, it is shown that collisional excitation from the $2s2p\,{}^3P$ level is dominant in this experiment, whereas inner-shell excitation from the $1s2p\,{}^3P$ level was dominant in two previous experiments using higher-Z He-like ions.[2,9] The present work represents the first evidence of excitation of the $2p^2\,{}^3P$ level primarily from the $2s2p\,{}^3P$ level, and the first experimental measurement of this collisional excitation rate between two doubly excited levels.

The space-resolved spectra from the plasma region near the carbon target are presented in Sec. II. The plasma parameters as functions of distance from the target are determined from the experimental data in Sec. III. These parameters include the electron temperature, electron density, and carbon ion densities for the three highest stages of ionization. A simple analytical expression for the relative intensity of the $2p^2\,{}^3P$-$1s2p\,{}^3P$ spectral line, as a function of nuclear charge Z and electron density, is derived in Sec. IV. The measured $2s2p\,{}^3P$-$2p^2\,{}^3P$ collisional rate coefficient agrees with the recent calculations of Sampson.[13] In Sec. V, it is shown that photoexcitation and electron collisional excitation from the $1s2p\,{}^3P$ level are unimportant in the plasma region near the target. Using the plasma parameters determined in Sec. III, the entire Lyman-α and satellite intensity distribution is numerically simulated in Sec. VI. Finally, in Sec. VII, the reliability of the $2p^2\,{}^3P$-$1s2p\,{}^3P$ satellite line for density measurements in dense laser-produced plasmas of varying Z is reconsidered in light of the present work. The time dependence of the plasma parameters and the validity of the steady-state numerical modeling are also discussed.

II. CARBON SPECTRA

The carbon plasma is produced by irradiating a graphite slab target with Nd-glass laser radiation (typically 4 J, 17 nsec) normal to the target surface as shown in Fig. 1. The focal spot is circular with a radius of approximately 300 μm. Using a 2.2 m grazing-incidence spectrometer with a gold-coated 600 grooves/mm grating (1.5° blaze angle, 87.5° angle of incidence), the carbon spec-

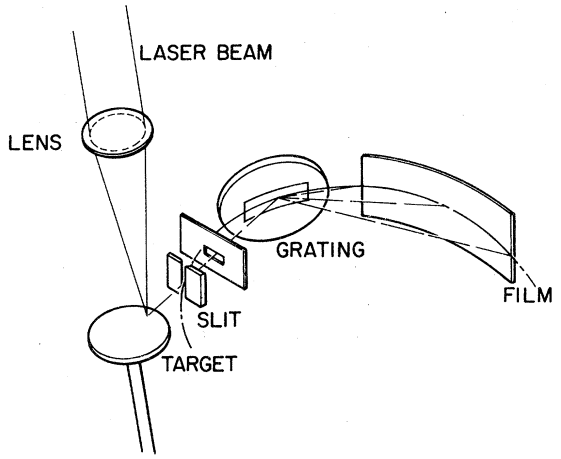

FIG. 1. Schematic of the experimental apparatus indicating the space-resolving aperture between the spectrometer entrance slit and the grating.

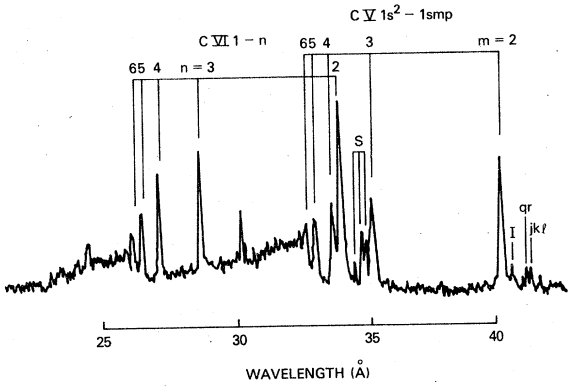

FIG. 2. Densitometer trace of the first-order spectrum, at a distance of 120 μm from the target, showing the C VI and C V resonance lines, the satellites (labeled *S*) of the C VI Lyman-α line, the satellites (*qr* and *jkl*) of the C V $1s^2$-$1s2p$ line, and the intercombination line (*I*).

trum is recorded on Kodak SWR emulsion. A 12 μm spectrometer entrance slit, oriented perpendicular to the target surface, results in a 90 mÅ instrumental spectral line width. Spatial resolution of 130 μm is provided by a 100 μm slit aligned parallel to the target surface. A useful film exposure is obtained with 160 laser shots, and the target disk is rotated to a new position before each shot. Time-dependent visible[14] and more recent soft x-ray data, obtained on single laser shots, indicate that the plasma is reproducible. The ambient pressure in the target chamber is less than 50 mtorr.

A film calibration (photographic density versus relative exposure) is determined from multiple exposures of spectra obtained using a varying number of laser shots. The photographic densities (typically 0.2) of the satellite lines and high-n resonance lines are in the portion of the calibration curve where the photographic density is linearly proportional to the relative exposure.

The carbon spectrum from the plasma region centered at a distance of 120 μm from the target is shown in Fig. 2. The dielectronic satellite lines of interest are labeled *S*. This spectral region is shown expanded in Fig. 3, where the satellite spectral lines are numbered according to the keys in Tables I and II.

The $2l2l'$ levels of C V are shown in Fig. 4, and the radiative transitions[15] from these levels are listed in Table I. Also listed in Table I are values for q, the calculated relative satellite intensities at low electron density (corona equilibrium), and r, the intensities at high density (Saha equilibrium). These intensities, which are further discussed in Sec. IV, are relative to the intensity of line No. 15 set equal to 100. The identification of the satellite features, made on the basis of measured wavelengths and relative intensities in the first and second order spectra (Fig. 3), is given in Table II. The estimated uncertainty in the satellite line wavelengths, which are measured with respect to the Lyman-α line at 33.735 Å, is ±0.01 Å. This uncertainty represents the deviation from the mean wavelengths, measured from densitometer traces at several distances from the

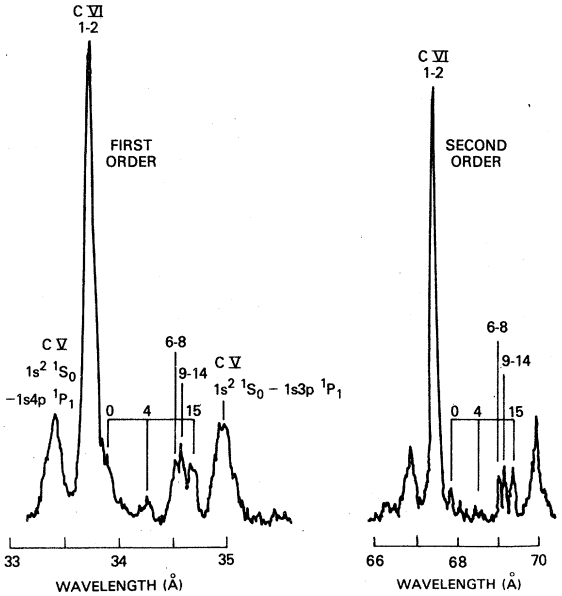

FIG. 3. Densitometer traces of the first- and second-order Lyman-α and satellite lines at 120 μm from the target. The identification numbers refer to the keys in Tables I and II.

TABLE I. The radiative transitions from the $2l2l'$ doubly excited levels of C V.

Key	Transition	λ (Å) [a]	A (10^{10} sec^{-1}) [a]	Γ (10^{12} sec^{-1}) [a]	q [b]	r [c]
1	$2p\,^2P_{3/2}$-$1s\,^2S_{1/2}$	33.732	81.0			46.6
2	$^2P_{1/2}$ $^2S_{1/2}$	33.737	81.0			23.3
3	$2p^2\,^1S_0$-$1s2p\,^1P_1$	33.884	108	14.3	14.4	15.5
4	$2s2p\,^1P_1$-$1s2s\,^1S_0$	34.312	75.3	202	32.0	32.0
5	$2p^2\,^1D_2$-$1s2p\,^3P_2$	34.377	0.0134	373	0.009	0.009
6	$2s2p\,^3P_2$-$1s2s\,^3S_1$	34.526	70.9	13.5	47.5	49.8
7	$^3P_1$ $^3S_1$	34.529	70.9	13.5	28.5	29.9
8	$^3P_0$ $^3S_1$	34.530	70.9	13.5	9.5	10.0
9	$2p^2\,^3P_2$-$1s2p\,^3P_1$	34.587	35.6	0.0459	0.79	25.0
10	$^3P_2$ $^3P_2$	34.588	106	0.0459	2.3	74.4
11	$^3P_1$ $^3P_1$	34.590	35.6	0.0	0.0	15.0
12	$^3P_1$ $^3P_0$	34.590	47.5	0.0	0.0	20.0
13	$^3P_1$ $^3P_2$	34.591	59.4	0.0	0.0	25.0
14	$^3P_0$ $^3P_1$	34.591	142	0.0024	0.03	19.9
15	$2p^2\,^1D_2$-$1s2p\,^1P_1$	34.709	143	373	100	100
16	$2p^2\,^3P_2$-$1s2p\,^1P_1$	34.925	0.0098	0.0459	0.0002	0.007
17	$^3P_1$ $^1P_1$	34.928	0.0011	0.0	0.0	0.0005
18	$2s^2\,^1S_0$-$1s2p\,^1P_1$	35.576	30.1	347	4.1	4.1

[a] Reference 15.
[b] Calculated using Eq. (14).
[c] Calculated using Eq. (16).

target, for the second order spectra where the satellite lines are well resolved. The spectral line at 33.943 Å is identified as the $2p3d\,^3F_4$-$1s3d\,^3D_3$ transition. This spectral line has been previously identified as the $2p3s\,^3P$-$1s3s\,^3S$ transition,[1,4,7] but this identification disagrees with the calculated wavelength (33.903 Å) and relative intensity listed in Ref. 16.

The dielectronic satellite spectra at three distances from the target are shown in Fig. 5. The intensity of the $2p^2\,^3P$-$1s2p\,^3P$ satellite line, relative to the $2s2p\,^3P$-$1s2s\,^3S$ line, is observed to decrease with distance.

III. MEASUREMENT OF PLASMA PARAMETERS

The measurement of the plasma parameters in the emission region near the target is necessary for the analysis of the satellite spectral lines. The relative importance of the competing population mechanisms of the $2l2l'$ doubly excited levels is determined primarily by the electron density and temperature. The plasma parameters are also important for the numerical modeling in the following sections.

TABLE II. Comparison of the measured and calculated wavelengths (in Å) for the satellite transitions identified in Fig. 3.

Key	Transition	Measured (±0.01 Å)	Theory [a]
0	$2p3d\,^3F_4$-$1s3d\,^3D_3$	33.943	33.941
4	$2s2p\,^1P_1$-$1s2s\,^1S_0$	34.280	34.312
6–8	$2s2p\,^3P_{0,1,2}$-$1s2s\,^3S_1$	34.545	34.527 [b]
9–14	$2p^2\,^3P_{0,1,2}$-$1s2p\,^3P_{0,1,2}$	34.603	34.589 [c]
15	$2p^2\,^1D_2$-$1s2p\,^1P_1$	34.712	34.709

[a] References 15 and 16.
[b] Blend of 34.526–34.530 Å.
[c] Blend of 34.587–34.591 Å.

The relevant plasma parameters (electron temperature, electron density, and ion densities) are obtained from various spectral line widths and intensity ratios. All of the plasma parameters at a particular distance from the target surface, determined by the spectrometer magnification at the film plane, are obtained from a single densitometer tracing over the wavelength range 10 to 90 Å. The plasma region of greatest interest, where the C V $2l2l'$ satellite lines are intense and where the high-density effects occur, is 100 to 200 μm from the target.

A. Electron temperature

Two radiative recombination continua, on the short-wavelength sides of the C VI and C V series limits, are present in the spectrum of Fig. 2. Electron temperatures, obtained from the slopes of these continua, are characteristic of the C VII and C VI plasma regions, respectively, wherein the next lower ionization stages are formed by radiative recombination. The dependence[17] of the continuum intensity I on wavelength is $\lambda^{-2}\exp(-hc/\lambda kT_e)$. Thus a graph of $\log(\lambda^2 I)$ as a function of λ^{-1} should approximate a straight line with slope equal

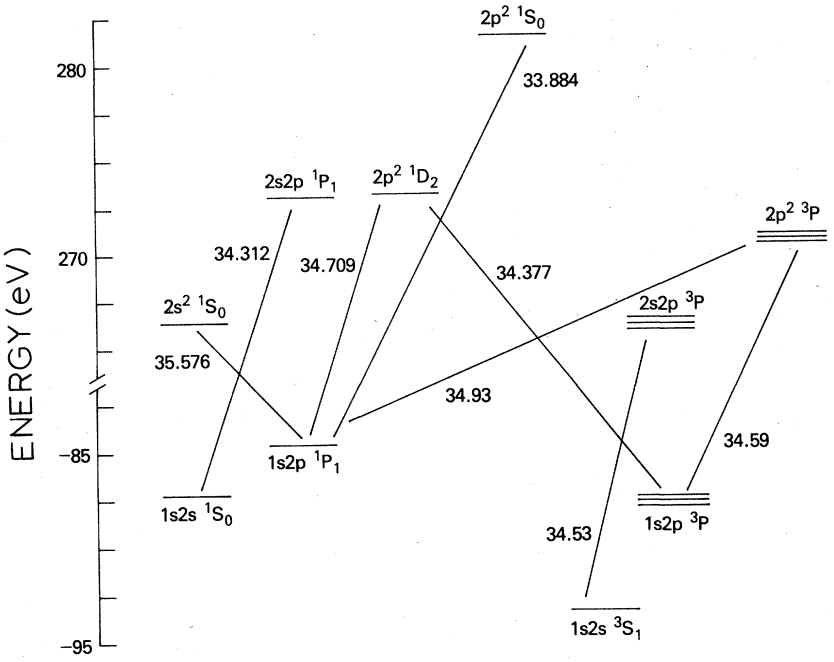

FIG. 4. The $2l2l'$ doubly excited levels of C V and the wavelengths of the strongest radiative transitions. The splitting of the triplet levels is not to scale.

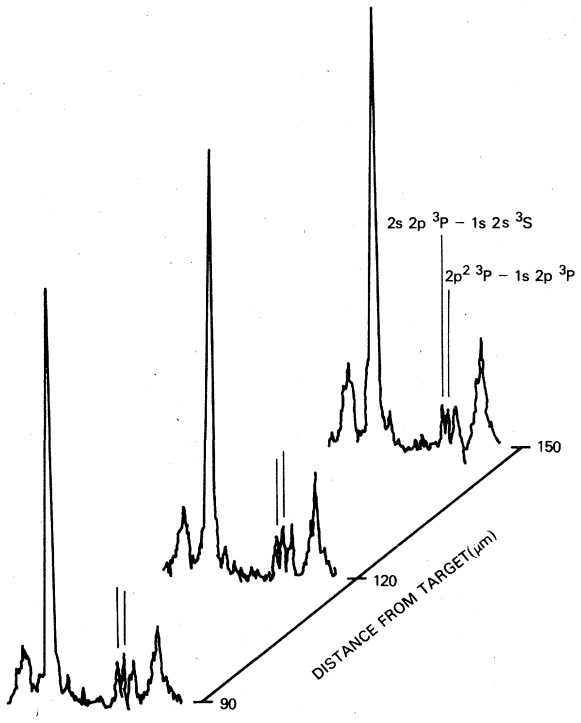

FIG. 5. Densitometer traces of the second order C VI Lyman-α and satellite lines at distances of 90, 120, and 150 μm from the target.

to $-hc/kT_e$.

A hydrogenic plasma is optically thin to recombination radiation if the density of ground-state absorbers, averaged along the line of sight, is less than[18] $2.6\times10^{16}\,Z^2\,\mathrm{cm}^{-2}$. Using $Z=6$ for carbon, the recombination radiation is unattenuated for C VI line-average densities less than 9×10^{17} cm^{-2}. It is shown below (Figs. 11 and 12) that the C VI and C V line-average densities are less than 3×10^{16} cm^{-2} so that absorption of the recombination radiation is negligible.

An uncertainty with this temperature measurement technique is the assignment of the background radiation level above which the recombination continuum intensity is measured. The C V continuum must be extrapolated to shorter wavelengths and subtracted from the C VI continuum.

The C VI and C V recombination intensities are digitized and processed numerically. A straight line is fitted to the C V $\log(\lambda^2 I)$ verses λ^{-1} data. Using the inferred temperature, the C V continuum is extrapolated to shorter wavelengths and subtracted from the C VI data. A straight line is then fitted to the resulting $\log(\lambda^2 I)$ versus λ^{-1} data, and the C VI temperature is determined. Shown in Fig. 6 are the temperatures for the spectrum at 120 μm (Fig. 2). As shown in Fig. 7, the electron temperatures decrease as functions of distance from the target.

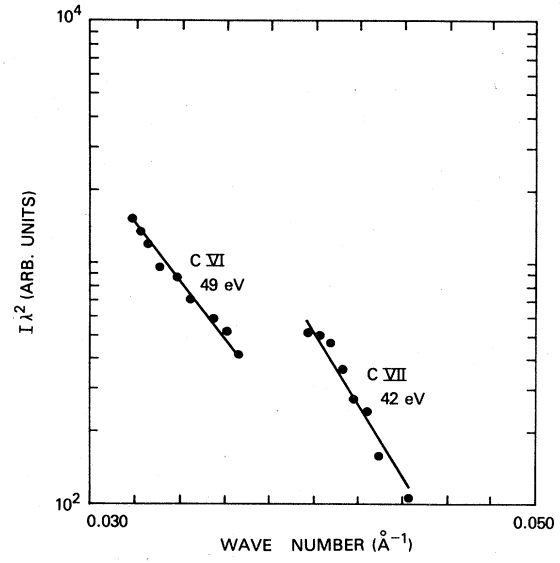

FIG. 6. The electron temperatures, determined from the slopes of the recombination continua at 120 μm from the target (Fig. 2), of the C VII and C VI plasma emission regions.

B. Electron density

The electron density is determined from the Stark broadening of the 26.357 Å C VI Lyman-δ 1–5 line in second order. Due to the absence of an unshifted central component, the Stark broadening of this spectral line in the high-density plasma near the target exceeds the Doppler and instrumental broadening. From the C VI ground-state densities determined below (Fig. 11), the opacity of the C VI 1–5 line is negligible.

The instrumental profile is obtained from the spectral lines far from the target where Stark and Doppler broadening are negligible. As shown in Fig. 8, the instrumental profile is nearly Gaussian in shape with a 90-mÅ linewidth which is attributable entirely to the effect of the 12-μm entrance slit of the spectrometer. Time-dependent data taken far from the target indicate that the C VI ions expand in a cone with a velocity of 2×10^7 cm/sec. Due to the small cone half-angle of 10°, the Doppler shifts resulting from the radial streaming motion of the ions are negligible.

The calculated Stark profiles, obtained by interpolation between tabulated profiles,[19] are convolved with the instrumental profile and are compared to the second order C VI 1–5 line as shown in Fig. 9. The Doppler broadening, when convolved with the Gaussian instrumental profile, is

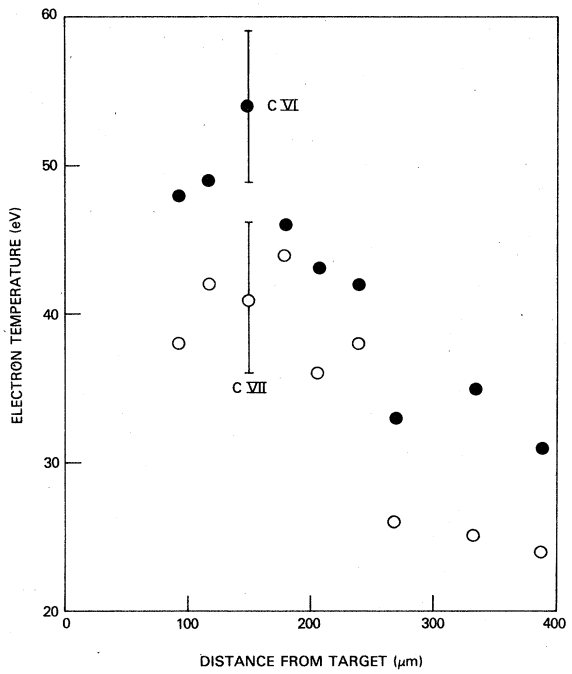

FIG. 7. The electron temperatures as functions of distance from the target for the C VI and C VII regions of the plasma.

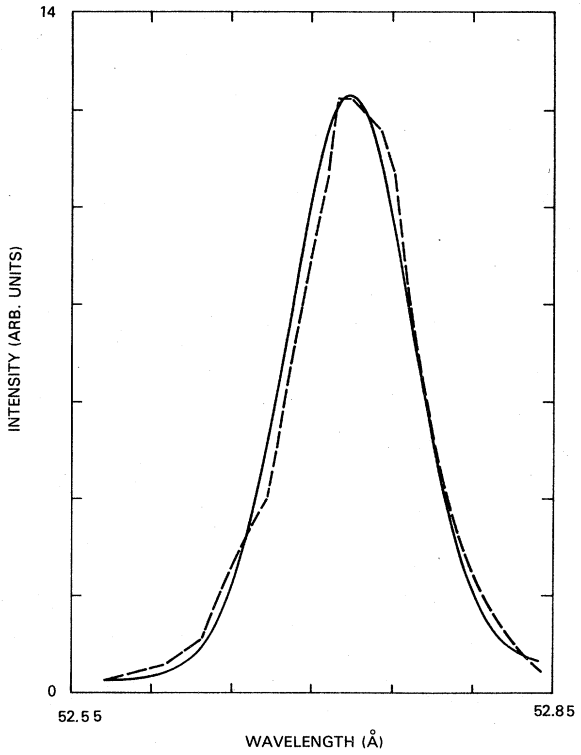

FIG. 8. A Gaussian profile (solid curve) is fitted to the second-order C VI 1–5 spectral line (dashed curve) at a distance of 360 μm from the target. The width of the instrumental profile (90 mÅ full width at half maximum) is due entirely to the 12 μm entrance slit of the spectrometer.

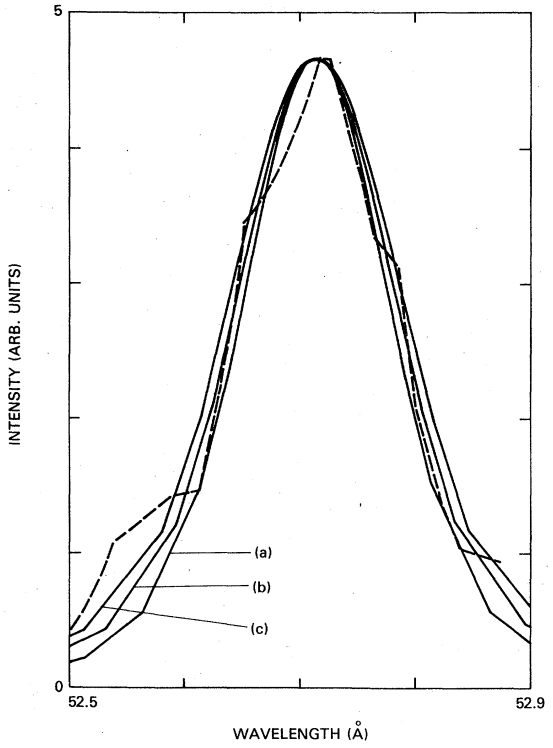

FIG. 9. The Stark profiles (Ref. 19), convolved with the instrumental profile, are fitted to the second-order CVI 1–5 spectral line (dashed curve) at a distance of 120 μm from the target. The calculated profiles are for electron densities (a) 1.0×10^{20} cm^{-3}, (b) 1.2×10^{20} cm^{-3}, and (c) 1.4×10^{20} cm^{-3}.

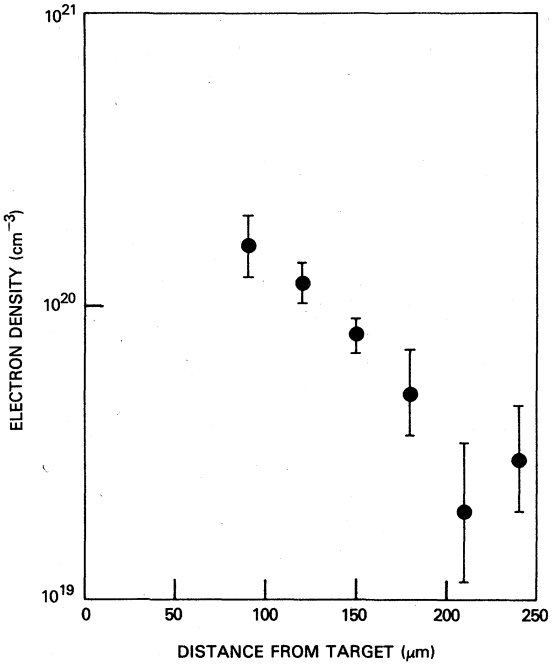

FIG. 10. The electron density, obtained from the Stark broadening of the second order CVI 1–5 spectral line, as a function of distance from the target.

negligible even near the target. The resulting electron density as a function of distance from the target is shown in Fig. 10. The uncertainty in the electron density measurement at 90 μm from the target is primarily due to the low line to background intensity ratio. The uncertainties at distances greater than 180 μm from the target are due to the weak dependence of the convolved profile on electron density.

C. Ion densities

The CVI ground-state density $\langle NR\rangle$, averaged over the line of sight R, is determined from the relative intensities of the CVI 1–4 and 1–5 spectral lines. In the high-density plasma region near the target, the higher hydrogenic levels are rapidly mixed by electron collisions. Two levels i and j are expected to be in equilibrium for an electron density[20]

$$N_e \geq 1.7\times10^{14}\, T_e^{1/2} E_{ij}^{\,3}\ \text{cm}^{-3}\,, \tag{1}$$

where T_e is the electron temperature and E_{ij} is the energy difference in eV. Using the electron temperatures and densities of Figs. 7 and 10, it is found that the CVI $n=4$ and 5 levels ($E_{45}=11.02$ eV) are in statistical equilibrium for distances within 300 μm of the target. If both the 1–4 and 1–5 transitions are optically thin, the ratio of the 1–4 intensity to the 1–5 intensity is

$$(g_4A_{41}/g_5A_{51})e^{E_{45}/T_e} = 1.92\, e^{11.02/T_e}\,.$$

Using the electron temperatures of Fig. 7, this ratio is in the range 2.4 to 2.8. The measured intensity ratios shown in Fig. 11 are smaller by a factor of two, and this difference is attributed to the opacity of these spectral lines in the dense plasma region near the target.

The optical depth at line center is[20]

$$\tau = (0.027\ \text{cm}^2/\text{sec}) f \langle NR\rangle/\Delta\nu\,, \tag{2}$$

where f is the oscillator strength, $\langle NR\rangle$ is the line-average density of the absorbing ground state, and $\Delta\nu$ is the spectral linewidth. The CVI 1–5 line has a large Stark width (53 mÅ at 120 μm from the target), whereas the Stark width of the 1–4 line, with a strong unshifted central component, is smaller than the thermal Doppler linewidth (5 mÅ). Thus the optical depth of the 1–4 transition, due to a smaller linewidth and larger oscillator strength, is much greater than the optical depth of the 1–5 transition. The measured intensity ratios for the CVI 1–4 and 1–5 lines are con-

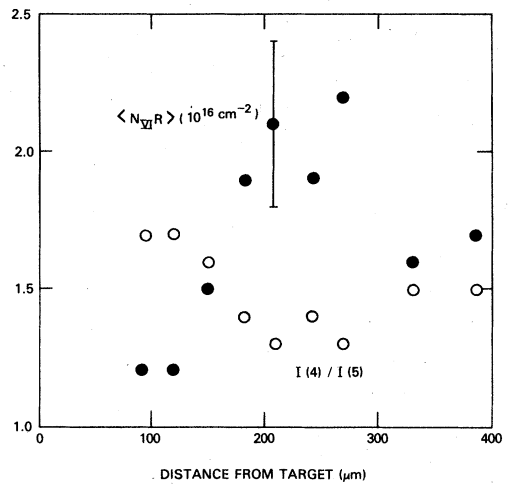

FIG. 11. The density of the C VI ground state, averaged over the line of sight, as obtained from the indicated intensity ratio of the C VI 1–4 and 1–5 spectral lines.

sistent with C VI 1–4 optical depths of order 1 and negligible 1–5 optical depths. Assuming that the reduction in the 1–4 to 1–5 intensity ratio is entirely accounted for by the escape factor[21] of the Doppler broadened 1–4 transition, the inferred values of the line-average density $\langle NR \rangle$ of the C VI ground state are shown in Fig. 11.

Using a similar procedure, the density of C V ground-state ions is obtained from the intensity ratio of the C V is $1s^2\,^1S_0$-$1s2p\,^1P_1$ resonance line and its *jkl* satellite lines[22] (identified in Fig. 2). These $1s^22p\,^2P$-$1s2p^2\,^2D$ satellite transitions terminate on an excited level of the C IV ion. Since the C IV ionization energy (64 eV) is comparable to the electron temperature near the target, the density of this ionization stage[23] and the optical depths of the satellite transitions are expected to be small due to rapid ionization. This is supported by the relatively weak C IV $1s^2\,2s$-$1s^2np$ spectral lines observed in the 212 to 312 Å wavelength region. Negligible satellite-line opacity is confirmed by noting that the intensities of the *jkl* and *qr* satellite lines (the latter terminating on the $1s^22s$ ground level) are equal in the spectrum of Fig. 2. This agrees with the intensity ratio of unity calculated for optically thin C IV satellite transitions.[24]

The C IV *jkl* satellite to C V resonance line ratio is a function of electron temperature and the opacity of the resonance line. By fitting analytical expressions to the optically thin tabulations of Ref. 24, we obtain

$$T_e = (0.709\ \text{eV})(Z-0.6)^{2.71}/[1+4.81\ \ln a/\ln(2000/b)]\,, \tag{3}$$

where

$$a = 2270 I_{jkl}/I_R c b^{2.08}\,, \tag{4}$$

$$b = Z-3\,, \tag{5}$$

$$N_e' = 7\times 10^5\,(Z-1)^{9.3}\,\text{cm}^{-3}\,, \tag{6}$$

and $c = 0.8$ if the electron density is greater than N_e' and $c = 1.0$ otherwise. Using $Z = 6$ and $c = 0.8$ for the present carbon experiment, Eq. (3) may be inverted to obtain the resonance-to-satellite line ratio as a function of temperature:

$$I_R/I_{jkl} = 1116\, e^{-92.5\ \text{eV}/T_e}\,. \tag{7}$$

Using the electron temperatures of Fig. 7, the intensity ratio should be in the range of 50–200. The measured intensity ratios shown in Fig. 12 are smaller by an order of magnitude. The reduced resonance-to-satellite line ratio is again attributed to the opacity of the resonance line. Assuming that the resonance line is primarily Doppler broadened and using the escape factor method of Ref. 21, the line-average density $\langle NR \rangle$ of the C V ground state is deduced as shown in Fig. 12.

The density of C VII ions is obtained from the intensity ratio of the higher (optically thin) C VI and C V resonance lines. Using Eq. (1), it may be shown that near the target the C VI $n = 5$ and the C V $1s5p\,^1P_1$ levels are in statistical (Saha) equilibrium[20] with the ground levels of the next higher ionization stages. Assuming equal electron density and temperature for the C VI and C V emitting regions, the C VII to C VI ion density ratio is

$$N_{VII}/N_{VI} = 0.24 e^{-6.1\ \text{eV}/T_e} I_{VI}/I_V\,, \tag{8}$$

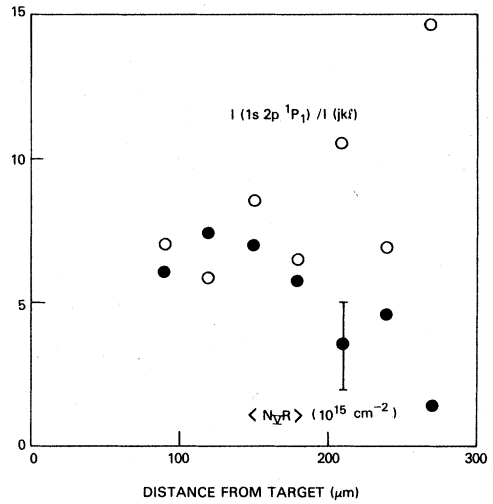

FIG. 12. The density of the C V ground state, averaged over the line of sight, as obtained from the indicated intensity ratio of the C V resonance line ($1s2p\,^1P_1$-$1s^2\,^1S_0$) and the *jkl* satellite-line blend.

where I_{VI} is the intensity of the C VI 5–1 transition and I_V is the intensity of the C V $1s5p\,^1P_1$-$1s^2\,^1S_0$ transition. From the measured intensity ratios of these two transitions, the C VII to C VI ion density ratio is found to be constant as a function of distance from the target and equal to 0.21 ± 0.03.

If the C VI and C V plasma regions are of approximately equal size, it is concluded from the analysis of the ion densities that the carbon ions are primarily in the hydrogen-like and helium-like ionization stages with comparable abundance. Comparing the values of $\langle NR \rangle$ from Figs. 11 and 12 with the electron densities of Fig. 10, the size of the highly ionized region of the plasma is of order 10 μm near the target. This is considerably smaller than the 300 μm radius of the focused laser beam. Since hot spots are observed in the burn pattern of the unfocused laser beam, the small size of the highly ionized plasma may be associated with nonuniform irradiation of the target.

IV. CALCULATED SATELLITE INTENSITY RATIO

The dielectronic satellite spectral lines, labeled S in Fig. 2, result from the radiative decay of the C V $2l2l'$ doubly excited levels shown in Fig. 4. These levels are normally populated by the dielectronic recombination process

$$C^{+5}(1s) + e \rightarrow C^{+4}(2l2l') , \tag{9}$$

in which an electron is captured into an excited state and another electron is simultaneously excited. The doubly excited levels may undergo autoionization, the inverse of Eq. (9), or may decay radiatively. Due to the shielding effect of the second electron, the wavelengths of the radiative transitions are slightly longer than the Lyman-α wavelength. The strongest $2l2l'$ satellite lines are well-resolved from the Lyman-α line.[15] The $2l3l'$ satellite lines, with the more highly excited spectator electron providing weaker shielding of the nucleus, generally lie closer to the Lyman-α line and are in most cases poorly resolved.[16]

Autionization of the $2p^2\,^3P_{0,1,2}$ levels is forbidden by the LS selection rule for parity, and the autoionization rates Γ listed in Table I are relatively low. The dielectronic recombination rates, obtained by detailed balancing from the autoionization rates, are also low for these levels. At high plasma densities, the population of the $2p^2\,^3P$ levels by electron collisional excitation from other levels of the ion becomes important, and the relative intensity of the 34.59 Å spectral radiation increases with density. The l-changing ($\Delta n = 0$) transition $2s2p\,^3P$-$2p^2\,^3P$ is normally the most rapid collisional process,[25] but collisional excitation from the $1s2p\,^3P$ level ($\Delta n = 1$) may also be important if the population of this excited level is large and if the electron temperature is sufficiently high to overcome the large energy difference.

It is shown in Sec. V that $\Delta n = 1$ photoexcitation and electron collisional excitation from the $1s2p\,^3P$ level are unimportant in this experiment. In the present section, it is assumed that each $2l2l'$ level is populated by electron collisional excitation from other $2l2l'$ doubly excited levels and by dielectronic recombination. The relative satellite intensities in the two limits of low and high electron densities are obtained. By neglecting spin-exchange excitation between the singlet and triplet levels, a simple analytical expression (reported earlier[26]) is obtained for the relative intensity of the $2p^2\,^3P$ satellite line as a function of electron density. The observed relative intensity of the $2p^2\,^3P$-$1s2p\,^3P$ line is then shown to be consistent with electron collisional excitation from the $2s2p\,^3P$ level.

The steady-state rate equations for the populations N_i of the ten $2l2l'$ levels shown in Fig. 4 may be written

$$D_i N_e N_H + N_e \sum_j C_{ji} N_j = N_i \left(\Gamma_i + \sum_k A_{ik} + N_e \sum_j C_{ij} \right) , \tag{10}$$

where $i,j = 1,2,3,\ldots,10$, N_H is the H-like ion ground-state density, N_e is the electron density, and C_{ji} is the electron collisional excitation rate coefficient. The radiative decay rates A_{ik} and the autoionization rates Γ_i have been calculated in Ref. 15 and are listed in Table I. The dielectronic recombination rate coefficient D_i is related to the autoionization rate by detailed balancing:

$$D_i = h^3 (2\pi m_e k T_e)^{-3/2} (g_i / 2g_H) \Gamma_i e^{-E_i / kT_e} , \tag{11}$$

where m_e is the electron mass, g_i is the statistical weight of the doubly excited level, $g_H = 2$ is the statistical weight of the H-like ion ground state, and E_i is the energy of the doubly excited level above the ionization limit of the He-like ion.

In the low-density limit, where electron collisional excitation is negligible, Eq. (10) has the simple solution

$$N_i = D_i N_e N_H / \left(\Gamma_i + \sum_k A_{ik} \right) . \tag{12}$$

Due to the exponential factor in the dielectronic recombination rate (11), the populations of the doubly excited levels are low when the electron temperature is much less than E_i. Indeed, in a laser-produced plasma, the dielectronic satellite lines are observable only in the high-temperature

region near the target.

The intensity of a radiative transition originating on level i and terminating on level f is $N_i h\nu_{if} A_{if}$. Using Eqs. (11) and (12), the ratio of two satellite lines is

$$I_{if}/I_{mn} = (q_{if}/q_{mn}) e^{-E_{im}/kT_e}, \tag{13}$$

where

$$q_{if} = g_i \Gamma_i A_{if}/\lambda_{if}\left(\Gamma_i + \sum_k A_{ik}\right) \tag{14}$$

and similarly for q_{mn}. The intensity ratio (13) is independent of electron density and is a weak function of electron temperature (since $E_{im} \ll kT_e$ in the hot plasma where the satellite lines are observable). The relative satellite intensities are proportional to q_{if}, whose values for C V are listed in Table I.

In the limit of high electron density, where radiative decay and autoionization are negligible compared to the collisional rates, the doubly excited levels are statistically populated. The ratio of the intensities of two satellite transitions is then

$$I_{if}/I_{mn} = (r_{if}/r_{mn}) e^{-E_{im}/kT_e}, \tag{15}$$

where

$$r_{if} = g_i A_{if}/\lambda_{if} \tag{16}$$

and similarly for r_{mn}. Again, the relative satellite intensities are independent of electron density and vary weakly with temperature. The relative intensities r_{if} are listed in Table I.

Comparing the value of q and the value of r for each satellite transition listed in Table I, it is apparent that the high-density relative intensity is significantly larger than the low-density intensity only for the transitions originating on the $2p^2\,^3P$ levels. Due to the small dielectronic recombination rates for these levels, the $2p^2\,^3P$ transitions are easily enhanced by electron collisional excitation from other energy levels.

By neglecting fine structure splitting and spin-exchange collisional excitation, which is a factor[13] of 40 slower than the triplet-triplet transiton, the rate equation (10) for the population N_1 of the $2s2p\,^3P$ level may be written

$$D_1 N_e N_H + N_e C_{21} N_2 = N_1(\Gamma_1 + A_1 + N_e C_{12}). \tag{17}$$

The equation for the population N_2 of the $2p^2\,^3P$ level is the same as Eq. (17), but with the subscripts 1 and 2 interchanged. The intensity for the group of blended satellite lines originating on level 2 is $N_2 \sum h\nu_{2f} A_{2f}$. After solving the rate equations for the level populations N_1 and N_2, the intensity I_2 of the $2p^2\,^3P$ transitions divided by the intensity I_1 of the $2s2p\,^3P$ transitions is[26]

$$\rho = \rho_0 + (\rho_s - \rho_0)/(1 + N_e^*/N_e), \tag{18}$$

where

$$\rho_0 = \beta \sum_f q_{2f} / \sum_n q_{1n}, \tag{19}$$

$$\rho_s = \beta \sum_f r_{2f} / \sum_n r_{1n}, \tag{20}$$

$$N_e^* = \beta D_1 (A_2 + \Gamma_2)/(D_1 + D_2) C_{12}, \tag{21}$$

$$\beta = e^{-E_{21}/kT_e}, \tag{22}$$

and $E_{21} = E_2 - E_1$ (4.8 eV for carbon). Since $E_{21} \ll kT_e$, $\Gamma_2 \ll A_2$, and $\Gamma_2 \ll \Gamma_1$, we set $\beta = 1$ and obtain, approximately,

$$N_e^* = A_2/C_{12}. \tag{23}$$

Using this last approximation results in a 1% error in the intensity ratio calculated from Eq. (18) for carbon and slightly higher errors for higher-Z He-like ions.

The intensity ratio (18) has a particularly simple form and is equal to ρ_0 at low electron density and ρ_s at high density. At the electron density N_e^*, the intensity ratio is equal to the average value $(\rho_0 + \rho_s)/2$, and the graph of ρ as a function of $\log N_e$ has its steepest slope. In order to observe the density variation of the $2p^2\,^3P$ satellite lines, the electron density should be of order N_e^*.

The total radiative decay rate for the $2p^2\,^3P$ level is

$$A_2 = 2.75 \times 10^9 Z^{4.1}\ \text{sec}^{-1}. \tag{24}$$

For temperatures in the range $10E_{21}$ to $100E_{21}$, where hydrogenic ions are prominent, the calculated[13] rate coefficient for the electron collisional transition $2s2p\,^3P$-$2p^2\,^3P$ has been fitted with the expression

$$C_{12} = \frac{4.73 \times 10^{-6}\ \text{cm}^3/\text{sec}}{(Z - 0.7)^2 T_e^{1/2}} \left(\frac{T_e}{E_{21}}\right)^{0.22}. \tag{25}$$

For the carbon $2s2p\,^3P$ radiative transitions 6 to 8 and the $2p^2\,^3P$ transitions 9 to 14 listed in Table I, $\rho_0 = 0.036$ and $\rho_s = 2.0$. Since all the paramaters in Eq. (18) are known, the observed ratio of the intensity of the 34.59 Å satellite line to the 34.53 Å line, measured as a function of electron density and temperature, may be compared with the theoretical expression with no adjustable parameters. As shown in Fig. 13, the observed intensity ratios are 10% higher than the calculated intensity ratios, but the agreement is within the experimental uncertainties of the electron density measurements.

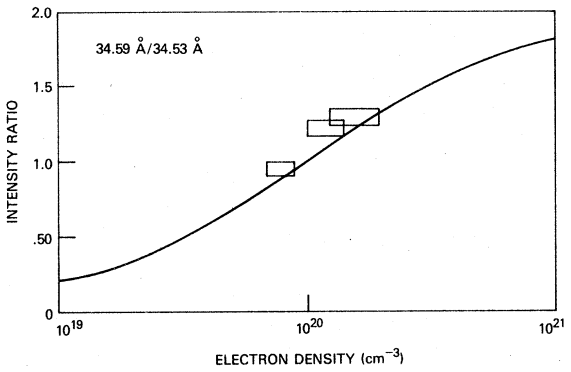

FIG. 13. Comparison of the calculated (curve) and the measured (boxes) intensity ratio for the C v 34.59 Å (transitions 9 to 14 in Table I) and 34.53 Å (transitions 6 to 8) satellite lines. The intensity ratios were measured from the second-order spectra at 90, 120, and 150 μm from the target (Fig. 5).

V. PHOTOEXCITATION AND INNER-SHELL EXCITATION

In addition to electron collisional excitation from the $2s2p\,^3P$ level considered in the previous section, population of the $2p^2\,^3P$ level by reabsorption of the satellite line radiation and by electron collisional excitation from the $1s2p\,^3P$ level must be considered. In this section, it is shown that such photoexcitation and collisional inner-shell excitation from the $1s2p\,^3P$ level are negligible in the present experiment. It is also shown that collisional excitation from the $1s2p\,^3P$ level was the dominant excitation mechanism in two previous measurements[2,9] of anomalously intense $2p^2\,^3P$ satellite radiation.

A. Photoexcitation

An estimate of the satellite line opacities is obtained from the measurement of the C V density. From Fig. 12, the line-average density $\langle NR\rangle$ of the C V ground state at a distance of 120 μm from the target is 7.4×10^{15} cm^{-2}. Assuming that the $1s2p\,^1P_1$ level is populated by electron collisional excitation from the ground state and depopulated by collisional deexcitation and radiative decay (reduced by the escape factor obtained from Fig. 12), the density of the $1s2p\,^1P_1$ level is a factor of 0.004 smaller than the ground-state density. The inferred optical depth of the $2p^2\,^1D_2$-$1s2p\,^1P_1$ satellite transition (No. 15 in Table I) is 0.02.

The calculated intensity of the $2s2p\,^3P$ radiation (transitions 6–8 in Table I), relative to the $2p^2\,^1D_2$ intensity, is nearly independent of electron density and temperature and is equal to 0.9. This agrees with the observed satellite intensities shown in Fig. 3. Since the $2p^2\,^1D_2$ satellite line is known to be optically thin and the observed relative intensity of the $2s2p\,^3P$ satellite radiation agrees with the optically thin value 0.9, we conclude that the $2s2p\,^3P$-$1s2s\,^3S$ radiation is unattenuated by opacity.

The oscillator strengths, averaged over the fine structure levels, for the $2p^2\,^3P$ (transitions 9 to 14 in Table I) and $2s2p\,^3P$ (transitions 6 to 8) radiation are 0.255 and 0.380. For statistically populated lower levels, the optical depth of the $2p^2\,^3P$ radiation is a factor of 2 greater than the optical depth of the $2s2p\,^3P$ radiation. Having shown that the optical depth of the $2s2p\,^3P$ radiation is negligible, the optical depth of the $2p^2\,^3P$ radiation must also be small.

The intensity of the $2s2p\,^1P_1$-$1s2s\,^1S_0$ transition in Table I, relative to the $2p^2\,^1D_2$-$1s2p\,^1P_1$ intensity, is independent of electron density and temperature and is equal to 0.32. Since this agrees with the observed intensity ratio (Fig. 3), the $2s2p\,^1P_1$ satellite line is unattenuated by opacity. Thus the four $2l2l'$ satellite lines identified in Fig. 3 are unattenuated by opacity. We conclude that population of the doubly excited levels by reabsorption of the satellite line radiation is unimportant in this experiment.

B. Inner-shell excitation

The inner-shell excitation process $1s2p\,^3P$-$2p^2\,^3P$, induced by electron collisions, is a possible excitation mechanism for the $2p^2\,^3P$ doubly excited level. The ratio of the inner-shell excitation rate to the $\Delta n=0$ excitation rate considered in the previous section is

$$R=C_{32}N_3/C_{12}N_1\,, \tag{26}$$

where the subscripts refer to $2s2p\,^3P$ (level 1), $2p^2\,^3P$ (level 2), and $1s2p\,^3P$ (level 3).

The inner-shell excitation rate coefficient may be written[24]

$$C_{32}=1.6\times10^{-5}f\bar{g}e^{-E_{23}/T_e}/E_{23}T_e^{1/2}\,, \tag{27}$$

where the energy difference in $10Z^2$ eV and the effective Gaunt factor is 0.2. Using the rate coefficient C_{12} given by Eq. (25),

$$R=0.017e^{-E_{23}/T_e}\left(\frac{E_{21}}{T_e}\right)^{0.22}\left(\frac{Z-0.7}{Z}\right)^2\frac{N_3}{N_1}\,. \tag{28}$$

The density ratio N_3/N_1 is obtained from the ratio of the intercombination line and $2s2p\,^3P$ satellite intensities:

$$N_3/N_1=3A_1\lambda_3I_3/A_3\lambda_1I_1\,, \tag{29}$$

where I_3 is the $1s2p\,^3P_1$-$1s^2\,^1S_0$ intercombination line intensity and I_1 is the $2s2p\,^3P$-$1s2s\,^3S$ satellite

intensity. The intercombination radiative rate[27] A_3 is $0.27Z^{10.3}$ sec^{-1} and the satellite radiative rate[15] A_1, averaged over the fine structure levels, is $4.57\times10^8Z^{4.1}$ sec^{-1}. The ratio of the inner-shell excitation rate to the $\Delta n=0$ excitation rate becomes

$$R = 8.6\times10^7 e^{-E_{23}/T_e}\left(\frac{E_{21}}{T_e}\right)^{0.22}\frac{(Z-0.7)^2}{Z^{8.2}}\frac{I_3}{I_1}. \quad (30)$$

For the present carbon experiment, the intensity ratio I_3/I_1 and the excitation ratio R are given in Fig. 14. Since R is small, inner-shell excitation of the $2p^2\,^3P$ level is small compared to the $\Delta n=0$ excitation from the $2s2p\,^3P$ level.

In the fluorine experiment of Ref. 2, the electron temperature was 340 eV and $I_3/I_1=2$. Thus $R=7$ and inner-shell excitation was the dominant collisional excitation mechanism. This explains why the $2p^2\,^3P$ satellite line was observable at an electron density of 5×10^{19} cm^{-3}, more than an order of magnitude lower than the density of Eq. (23) based on $2s2p\,^3P$-$2p^2\,^3P$ excitation alone.

Using the magnesium data of Refs. 9 and 28, the electron temperature was 250 eV and $I_3/I_1>20$. Thus $R>0.5$ and inner-shell excitation contributed significantly to the $2p^2\,^3P$ population. This resulted in an overestimation[9] of the $2s2p\,^3P$-$2p^2\,^3P$ excitation rate coefficient by a factor of 3 compared to the value obtained from Eq. (25).

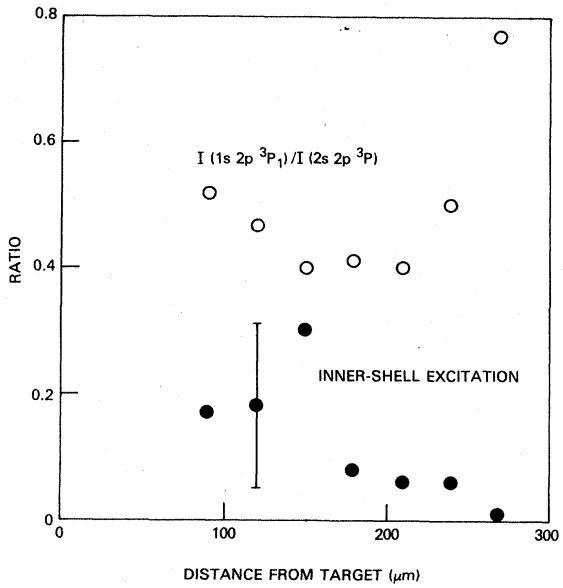

FIG. 14. The inner-shell excitation rate, relative to the $\Delta n=0$ excitation rate, as obtained from the indicated intensity ratio of the C V intercombination line ($1s2p\,^3P_1$-$1s^2\,^1S_0$) and the $2s2p\,^3P$-$1s2s\,^3S$ satellite line.

VI. NUMERICAL SIMULATION

In deriving the analytical intensity ratio of Eq. (18), only dielectronic recombination and allowed dipole collisional population of the $2p^2\,^3P$ level were considered. The results are valid for electron densities of magnitude less than a factor of 10 times the densities of Eq. (23), about 10^{21} cm^{-3} for C V. At higher densities, spin-exchange transitions and recombination from the hydrogenic $n=2$ level become important.[10] The complete set of coupled rate equations, including all of these processes, has been solved for the $2l2l'$ level populations and the satellite-line intensities. This numerical model permits the simulation of the observed satellite intensity spectra shown in Fig. 3. The intensities of the satellite transitions listed in Table I are calculated, and linewidths are included to simulate instrumental, Doppler, and Stark broadening. The calculated intensity distribution as a function of wavelength may be compared directly with the observed spectrum.

In this section, the numerical model will be described in general terms. A detailed description, including simulation of the high-density spectra of higher-Z ions, will be given in a separate publication.

The steady-state rate equations for the ten $2l2l'$ levels (see Fig. 4), the three hydrogenic $n=2$ sublevels, and the fully stripped ionization stage are solved numerically for the level populations relative to the hydrogenic ground state density. These levels are coupled by electron collisional processes (dielectronic recombination, collisional-radiative recombination, ionization, and excitation) and by autoionization and radiative decay where appropriate. The optically thick Lyman-α radiative rate is reduced by the escape factor.[21] Since the satellite lines are assumed to be optically thin and inner-shell excitation is neglected, the $2l2l'$ doubly excited levels are not coupled to the He-like singly excited levels. This last approximation may be verified on a case-by-case basis as described in the previous section.

The satellite transition wavelengths, autoionization rates, and radiative decay rates of Ref. 15 are used. The rate coefficients for electron collisional transitions among the $2l2l'$ levels have recently been calculated by Sampson.[13] Approximate hydrogenic expressions are used for collisional-radiative recombination and ionization of the $2l2l'$ levels. These latter two collisional processes, though unimportant in the present carbon experiment, become dominant in the limit of extremely high densities, and more accurate atomic rates are currently being calculated.[13]

Having calculated the level populations, the

spectral intensity distribution is simulated by summing the contributions from each radiative transition at particular wavelengths in a wavelength region that includes the Lyman-α and satellite lines. The Doppler, Stark,[19] and instrumental (Fig. 8) profiles are convolved, and the Lyman-α profile is further modified for opacity. The calculated spectral distribution is a function of the electron density, temperature, line-average density $\langle NR \rangle$ of the hydrogenic ground state, and instrumental width. Since all of these parameters have been measured independently of the Lyman-α and satellite lines, the calculated spectrum may be compared to the observed spectrum with no adjustable parameters. Except for the Lyman-α line, there is good agreement between the calculated spectra of Fig. 15 and the observed spectra of Fig. 3. The calculated Lyman-α intensity may be brought into agreement with the measured intensity by altering the temperature and opacity by 10%, which is within the uncertainties of the measured values. While transport of the Lyman-α radiation could be treated using a more sophisticated numerical model, the simple escape factor approximation results in agreement with the observed Lyman-α profile within the uncertainty of the measurements.

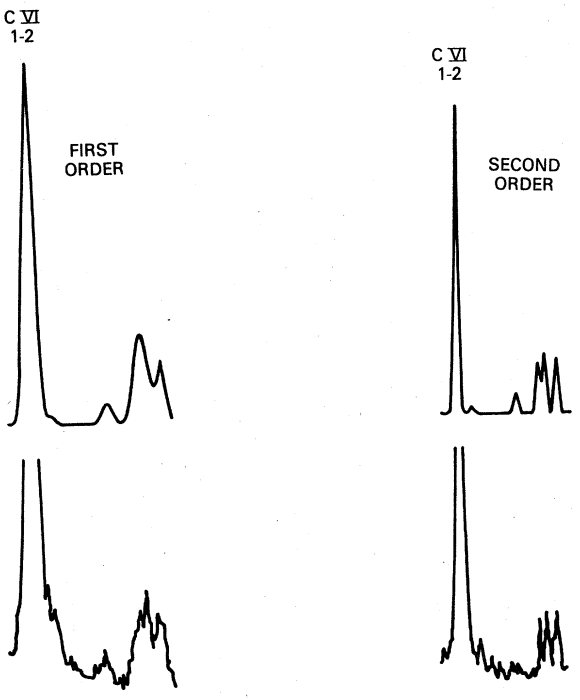

FIG. 15. The Lyman-α and satellite intensity distributions at 120 μm calculated using the measured electron density 1.2×10^{20} cm^{-3}, line-average C VI ground-state density $\langle NR \rangle = 1.2\times10^{16}$ cm^{-2}, and temperature 49 eV (upper curves). Instrumental widths of 90 mÅ (left spectrum)and 45 mÅ (right) have been added to the intensity distributions. These calculated spectra may be compared directly with the observed first- and second-order satellite spectra (Fig. 3) which are shown below the calculated spectra.

The $2l3l'$ levels are not included in the numerical model, and the $2p3d\,^3F$ line (labeled 0 in Fig. 3) does not appear in the calculated spectrum. It is likely that the base of the Lyman-α line in Fig. 3, particularly on the long-wavelength side, is broadened by unresolved $2l3l'$ lines.

Visual inspection of the film plate indicates that the $2s2p\,^3P$ (transitions 6 to 8 in Table I) and $2p^2\,^3P$ (9 to 14) satellite lines are resolved in first order (see Fig. 3). These two satellite lines are not resolved in the first-order calculated spectrum probably due to slight errors in the theoretical wavelengths (Table II).

VII. DISCUSSION

It was shown in the previous section that, given the plasma parameters and the instrumental width, the Lyman-α and satellite intensity distribution may be accurately simulated. The relative intensity of the $2p^2\,^3P$ satellite line is a strong function of electron density, and the relative intensity of the Lyman-α line is a strong function of temperature and opacity. Given a Lyman-α and satellite spectrum, it is possible to determine the electron density and either the temperature or the opacity of the source plasma.

This diagnostic technique, which depends on the relative intensities of the spectral lines, has several advantages over the more traditional line broadening diagnostics. Since the satellite lines terminate on excited levels, they are less susceptible to opacity than the Lyman series resonance lines, but satellite line opacity may be important at high densities.[29] In any case, the absence of satellite line opacity may be established using the procedures of Sec. V.

The occurrence of electron collisional excitation of the $2p^2\,^3P$ level from the $1s2p\,^3P$ level, if comparable to the excitation from the $2s2p\,^3P$ level, will enhance the $2p^2\,^3P$ satellite intensity and mimic the high-density effect. This is most likely to occur when the metastable population and the electron temperature are relatively high as in the case of a transiently ionizing plasma. Since the metastable population may depend on the time history of the plasma as well as the local plasma parameters, the interpretation of the $2p^2\,^3P$ satellite intensity is simpler if the presence of inner-shell excitation can be ruled out as was done for the present experiment in Sec. V.

Due to the transient nature of laser-produced

plasmas, the validity of the steady-state rate equation analysis must be considered. For the case of carbon targets irradiated by laser pulses with durations in the range 4.5 to 17 nsec, it has been shown that a stationary electron density profile is established during the laser pulse.[30-33] The electron density, measured from time-integrated spectroscopic data, is a good representation of the stationary density that exists during the laser pulse, with small errors due to the transient buildup and decay of the plasma. The electron temperature follows the rise and fall of the laser intensity,[32] and the measured temperature is an average over the duration of the laser pulse. As shown by Eq. (11) and (12), the absolute satellite emission is cut off by an exponential factor at low electron temperatures, and the strongest satellite emission has been observed to occur near the peak of the laser pulse.[34,35] Thus the time-integrated satellite data are characteristic of the plasma conditions that exist near the peak of the laser pulse. Since the relative satellite intensities depend strongly only on the electron density, which is stationary when the satellite emission occurs, the steady-state rate equation analysis is appropriate.

It has been shown that the carbon dielectronic satellite lines are a promising diaganostic for plasmas with electron densities 10^{19} to 10^{21} cm^{-3}. This density range may be extended by using higher-Z ions. For example, ablative laser fusion targets are presently coated with a fluorocarbon plastic. Using the C V and F VIII satellite lines, it should be possible to measure electron densities in the ablation plasma in the range 10^{19} to 10^{22} cm^{-3} if the spatial resolution is adequate to resolve the high-density emitting region.

ACKNOWLEDGMENTS

We thank Hans R. Griem for useful comments on the manuscript. We also thank James L. Ford for expert technical assistance. This work was supported in part by the U. S. Department of Energy.

[1]Uri Feldman and Leonard Cohen, Astrophys. J. 158, L169 (1969).
[2]U. Feldman, G. A. Doschek, D. J. Nagel, W. E. Behring, and R. D. Cowan, Astrophys. J. 187, 417 (1974).
[3]U. Feldman, G. A. Doschek, D. J. Nagel, and R. R. Whitlock, Astrophys. J. 192, 213 (1974).
[4]R. D. Cowan, N. J. Peacock, M. G. Hobby, and M. Galanti, J. Phys. B 6, L298 (1973).
[5]E. V. Aglitskii, V. A. Boiko, L. A. Vainshtein, S. M. Zakharov, O. N. Krokhin, and G. V. Sklizkov, Opt. Spektrosk. 35, 963 (1973) [Opt. Spectrosc. (USSR) 35, 557 (1973)].
[6]E. V. Aglitskii, V. A. Boiko, S. M. Zakharov, S. A. Pikuz, and A. Ya. Faenov, Kvant. Elektron. (Moscow) 1, 908 (1974) [Sov. J. Quantum Electron. 4, 500 (1974)].
[7]Piergiorgio Nicolosi and Giuseppe Tondello, J. Opt. Soc. Am. 67, 1033 (1977).
[8]V. I. Bayanov, V. A. Boiko, A. V. Vinogradov, S. S. Gulidov, A. A. Ilyukhin, V. A. Katulin, A. A. Mak, V. Yu. Nosach, A. L. Petrov, G. V. Peregudov, S. A. Pikuz, I. Yu. Skobelev, A. D. Starikov, A. Ya. Faenov, V. A. Chirkov, and E. A. Yukov, Zh. Eksp. Teor. Fiz. Pis'ma Red. 24, 352 (1976) [JETP Lett. 24, 319 (1976)].
[9]A. V. Vinogradov, I. Yu. Skobelev, and E. A. Yukov, Zh. Eksp. Teor. Fiz. 72, 1762 (1977) [Sov. Phys. JETP 45, 925 (1977)].
[10]A. V. Vinogradov and I. Yu. Skobelev, Zh. Eksp. Teor. Fiz. Pis'ma Red. 27, 97 (1978) [JETP Lett. 27, 88 (1978)].
[11]John F. Seely, Phys. Rev. Lett. 42, 1606 (1979).
[12]J. F. Seely, R. C. Elton, and R. H. Dixon, Bull. Am. Phys. Soc. 24, 768 (1979).
[13]D. H. Sampson (private communication).
[14]R. H. Dixon and R. C. Elton, Phys. Rev. Lett. 38, 1072 (1977).
[15]L. A. Vainshtein and U. I. Safronova, At. Data Nucl. Data Tables 21, 49 (1978).
[16]L. A. Vainshtein and U. I. Safronova, in *Spectroscopic Constants of Atoms* (Spectroscopic Council of the USSR Academy of Sciences, Moscow, 1977).
[17]R. C. Elton, NRL Report No. 6738 (unpublished).
[18]J. Cooper, in *Reports on Progress in Physics*, edited by A. C. Stickland (Institute of Physics, London, 1966), Vol. XXIX.
[19]Hans R. Griem, Milan Blaha, and Paul C. Kepple, Phys. Rev. A 19, 2421 (1979); see also Naval Research Laboratory Report No. 3634, 1978 (unpublished).
[20]Hans R. Griem, *Plasma Spectroscopy* (McGraw-Hill, New York, 1964).
[21]R. W. P. McWhirter, in *Plasma Diagnostic Techniques*, edited by R. H. Huddlestone and S. L. Leonard (Academic Press, New York, 1965).
[22]V. L. Jacobs and M. Blaha, Phys. Rev. A 21, 525 (1980).
[23]D. Colombant and G. F. Tonon, J. Appl. Phys. 44, 3524 (1973).
[24]C. P. Bhalla, A. H. Gabriel, and L. P. Presnyakov, Mon. Not. R. Astron. Soc. 172, 359 (1975).
[25]Jon C. Weisheit, J. Phys. B 8, 2556 (1975).
[26]John F. Seely, Bull. Am. Phys. Soc. 24, 996 (1979).
[27]C. Laughlin, J. Phys. B 11, L391 (1978).
[28]G. V. Peregudov, E. N. Ragozin, and V. A. Chirkov, Kvant. Elektron. (Moscow) 2, 1844 (1975) [Sov. J. Quantum Electron. 5, 1012 (1976)].
[29]D. Duston and J. Davis, Phys. Rev. A 21, 932 (1980).
[30]H. Puell, Z. Naturforsch. 25a, 1807 (1970).
[31]H. Puell, H. J. Neusser, and W. Kaiser, Z. Naturforsch. 25a, 1815 (1970).
[32]H. Puell, W. Spengler, and W. Kaiser, Phys. Lett.

37A, 35 (1971).
[33]M. Galanti and N. J. Peacock, J. Phys. B 8, 2427 (1975).
[34]M. H. Key, C. L. S. Lewis, and M. J. Lamb, Optics Commun. 28, 331 (1979).
[35]M. H. Key, C. L. S. Lewis, J. G. Lunney, A. Moore, and J. M. Ward, Phys. Rev. Lett. 44, 1669 (1980).